Geochemical Investigation of Tanezzuft Formation, Murzuq Basin, Libya*

Tarek Hodairi[1] and Paul Philp[1]

Search and Discovery Article #10344 (2011)
Posted August 8, 2011

*Adapted from expanded abstract presentation at AAPG Annual Convention and Exhibition, Houston, Texas, USA, April 10-13, 2011

[1]School of Geology and Geophysics, University of Oklahoma, Norman, OK (hoderi75@ou.edu)

Abstract

A geochemical analysis was carried out on representative shale samples from the Uppermost Silurian Tanezzuft Formation ('cool' shale) in the Murzuq Basin, Libya, using methods including Rock-Eval pyrolysis (RE), gas chromatography (GC) and gas chromatography-mass spectrometry (GCMS). The distribution of the n-alkanes, isoprenoids, terpanes, and steranes have been studied and used to determine the types of organic matter, levels of thermal maturity, and nature of depositional environments. The results reveal that organic matter (OM) in the samples is characterized as being poor to fair in TOC. This is due to the relative oxicity of the depositional environment and/or most of the hydrocarbons have already been generated and migrated away from the source rock.

The samples are shown to be mainly Type III kerogen (gas prone) with some contribution of mixed type II and III kerogens (gas/oil prone). The predominance of nC_{17} over nC_{25} ratios in the n-alkanes profiles indicates a high input of marine-derived organic matter, if this is not related to maturation. Nonetheless, values of $Pr/_nC_{17}$ vs. $Ph/_nC_{18}$ indicate that OM in these sediments has mixed marine/terrigenous sources. This is further supported by a predominance of C_{27} and C_{29} steranes in most of the samples. Depositional environments of these sediments were determined to be mixed oxic to sub-oxic (high Eh) conditions as suggested by high ratios of Pr/Ph, the relative high concentrations of C_{30}-diahopane in some samples, and low ratios of C_{35} to C_{34} homohopanes as well as low quality organic matter (e.g. organic matter with low hydrogen index). The presence of pregnane and homopregnane could be related to hypersaline sedimentation conditions. Thermal maturity parameters including the sterane isomerization ratios $C_{29}\alpha\beta\beta/(\alpha\beta\beta+\alpha\alpha\alpha)$, $C_{29}\alpha\alpha\alpha 20S/(20S+20R)$, homohopanes isomerization ratio $C_{32}22S/(22S+22R)$, and C_{30}-moretanes/C_{30}-hopanes ($C_{30}\beta\alpha/C_{30}\alpha\beta$) ratio, together with Rock Eval data, support the early to intermediate maturity levels of studied rock samples. Therefore, it cannot be expected that the Uppermost Silurian Tanezzuft Formation ('cool' shale) has generated, or will generate, considerable amounts of hydrocarbons in the Murzuq Basin.

Introduction

The study area is situated within the Murzuq Basin of Southwest Libya. Murzuq Basin is one of a number of intracratonic basins located on the North African Saharan Platform. It covers an area of about 350,000 Km^2 in southwest of Libya and extends southwards into Niger where it is known as the Jadu Basin (Figure 1). The Murzuq Basin was subject to several compressional and extensional tectonic phases. These tectonic activities began during the Pre-Cambrian orogenesis that formed vertical basement faults, trending N-S, and counterbalanced by conjugated faults trending in a NE SW direction (Bellini and Massa, 1980; Echikh, 1998; Yahia et al., 2000). The Pan- African movements were followed by three principal tectonic episodes, including the Caledonian orogeny (Wenlokian, Late-Early Silurian), Hercynian orogeny that corresponds to the second major tectonic phase which has affected the Palaeozoic (Middle to Upper Carboniferous). This orogeny has caused folding, faulting and strong subsidence (Bellini and Massa, 1980). The third phase was the Alpine orogeny of the Tertiary period (Figure 2). According to Echikh and Sola (2000), there are seven major tectonic elements have been identified within Murzuq Basin from west to east, these are the Tihemboka Arch, Alawaynat Trough, Tirinine High, Awbari Trough, Idhan Depression, Brak-Bin Ghanimah uplift and Dur Al Qussah Trough (Figure 1). During the Mesozoic era (Jurassic time), the eastern rim of the basin was lifted and since then the Dur El Qussah has been a mountain chain (Yahia et al., 2000). Several folded units were located along the major N-S Tihemboka Arch in the western part of the basin (Figure 1), these folds were separated the Murzuq Basin (SW) and Ghadamis Basin (NE) in Libya from Illizi Basin in Algeria (SE).

The Palaeozoic sediments within the basin comprise Cambrian, Ordovician, Silurian, Devonian and Carboniferous rocks, and are unconformably overlain by up to 1500 m of Mesozoic continental deposits and Cainozoic sequences (Figure 2). The maximum depth to Precambrian basement reaches as much as 3500 m in the central part of the basin (Aziz, 2000). However, the Tanezzuft Formation (early-Llandoverian) consists of dark gray to black graptolitic shales with intercalations of siltstone and fine grained sandstones often forming rhythmical alternation; it represents the broad marine transgression of the Silurian sea over the North African craton.

In the Southwestern Murzuq Basin, the Tanezzuft Shale is about 475 meter thick, whereas in the subsurface it ranges from 45 to 300 meter. The basal Tanezzuft Formation (Lowermost) is recognized as radioactive hot shale and has a high gamma ray response in wireline logs. This is most probably due to the high content of uranium within the Tanezzuft Shale (Fello et al., 2006). The Lowermost Silurian Tanezzuft Formation (‘hot’ shale) and Middle-Late Devonian Awaynat Wanin Formation shale are thought to be the main source rocks (Echikh and Sola, 2000; Sikander et al., 2000) along with other local source rocks. These have been recognized within Palaeozoic sequences (Figure 2), and have contributed to charging of the Palaeozoic and Mesozoic reservoirs in the Murzuq Basin (Sikander et al., 2000; Yahia et al., 2000; Lüning et al., 2000d). Only one effective petroleum system (Tanezzuft-Mamuniyat) has been found in the Murzuq Basin to date, although others may remain to be discovered (Hallett, 2002).

Results and Discussion

Origin of Organic Matter and Depositional Conditions

It appears from Rock Eval results that the studied samples are generally poor to fair in TOC with values ranging from 0.40% to 1.28% (Figure 3 and Table 1). S1 values are also shown to be generally poor to fair with values ranging from 0.21 to 1.27 mg of HC/g (Table1). In contrast, only sample A6b has an excellent value of 10.59 mg of HC/g. However, these relatively low values of TOC and S1 could be related to the relative oxic depositional conditions of these samples (Jarvie, 1991; Peters et al., 1993) as strongly suggested by the high values of Pr/Ph ratios, the presence of C_{30}-diahopane, and the low ratios of C_{35} to C_{34} homohopanes, which all suggest mixed oxic to suboxic depositional conditions. This conclusion is further supported by fair potential S2 values for most of studied samples ranging from 0.38 to 1.82 mg of HC/g of rock (Table 1), thus, it is clear that the remaining hydrocarbon potential of these samples is very low. A crossplot of S2 vs. TOC (Figure 3) was used to determine the hydrocarbon potential for the samples in this investigation. Most of the samples were plotted in the poor and fair zones, and a few of them show good to excellent source rock quality and potential. Such large variation in samples may be due to variability and heterogeneity of kerogen in the different organic facies. The other S2 vs. TOC crossplot (Figure 4) was used to determine the type of kerogen and consequently the product type. The majority of the samples were shown to be Type III kerogen, which is characterized by low HI and high OI derived from terrestrial plant debris and/or aquatic organic matter deposited in an oxidizing environment that produces mainly gas (Tissot et al., 1974). A small contribution of mixed type II and III kerogens (gas/oil prone) is also observed in these samples.

The n-alkanes are generally in the C_{13}-C_{27} range, and typically maximize at n-C_{16} or n-C_{17} (Table 2; Figure 5). The predominance of nC_{17} over nC_{25} (Table 2) in all of the samples analyzed may suggest a high input of marine-derived organic matter, but this may result from maturation (Eglinton and Hamilton, 1969; Philp, 1985; Huang et al., 1999b). However, most of samples have Pr/Ph ratios greater than 1 (> 1) ranging between 1.23 and 2.32, except for sample A6b which shows a value of 0.96 (Table 2). This may be due to the variations in depositional conditions of source material (Didyk et al., 1978; Peters and Moldowan, 1993). The slight variation of Pr/Ph ratios from 1.23 and 2.32, suggests that the samples were deposited in mixed oxic to sub-oxic conditions. However, pristane/phytane ratios are known to be affected by maturation (Tissot and Welte, 1984) and by differences in possible precursors (Volkman and Maxwell, 1986; ten Haven et al., 1987). Another crossplot of $Pr/_nC_{17}$ vs. $Ph/_nC_{18}$ (Figure 6) was used to determine the organic matter input (c. f. Lijmbach, 1975; Shanmugam, 1985). Most of samples plotted appear in the region of mixed marine/terrigenous sources, which is consistent with the interpretations of n-alkane profiles (Figure 5), Rock-Eval data (Figure 4), and the predominance of C_{27} and C_{29} steranes in most of the samples (Figure 7 and Figure 8).

The distribution of C_{27}, C_{28} and C_{29} regular steranes for Tannezuft Formation samples are scattered over a wide area between C_{27} and C_{29} of the ternary diagram (Figure 7). The predominance of C_{27} and C_{29} steranes in most of the samples (Table 3) is interpreted as strongly indicate of a marine phytoplankton and terrestrial input respectively.

High values of diasterane/sterane ratios (Table 3) could result from samples having been deposited under highly oxic conditions and/or due to clay catalysis (Clark and Philp, 1989; Moldowan et al., 1992). This conclusion is relevant to the interpretation of high Pr/Ph ratios, relatively low values of TOC and S1, the presence of C_{30}-diahopane, and the low ratios of C_{35} to C_{34} homohopanes, which all designate mixed oxic to suboxic depositional conditions.

Low ratios of C_{35} to C_{34} homohopanes (0.38-0.65) in all samples (Table 4) suggest prevailing oxic to sub-oxic (high Eh) conditions during deposition (Peters and Moldowan, 1993) as further indicated by the low quality organic matter (e.g. organic matter with low hydrogen index; Dahl et al., 1994), high Pr/Ph ratios, the presence of C_{30}-diahopane, and high values of diasterane/sterane ratios for all samples.

The presence of pregnane, homopregnane (Figure 8), and C_{24} tetracyclic terpane (Figure 9) may be related to hypersaline sedimentation conditions (ten Haven et al., 1988). The widespread occurence of tricyclic terpanes in most of the samples (Table 4 and Figure 9) could be more related to marine influenced depositional conditions rather than maturity effect since most of the samples are at early to intermediate maturity levels (Siefert and Moldowan, 1979; Philp et al., 1992; Peters et al., 2005).

Evaluation of Thermal Maturation

On the basis of Tmax, the majority of samples have Tmax values in the range of 435 and 445°C indicating that the organic matter has reached the early to intermediate stages of thermal maturity (Figure 10 and Figure 11).

The values of 22S/(22S+22R) Homohopane isomerization of C_{32} homohopane for samples studied range from 0.48 0.75 (Table 4 and Figure 9) suggesting that the main stage of oil generation has been reached. This interpretation is further supported by the low values of the C_{30}-moretane/C_{30}-hopane ($C_{30}\beta\alpha/C_{30}\alpha\beta$) ratios (0.11-0.35) for all samples. Usually this ratio decreases with increasing thermal maturity from 0.8 in immature source rock to values of less than 0.15 in mature stages (Rullkötter and Marzi, 1988; Peters and Moldowan, 1993). Since the samples are at early to intermediate stages of thermal maturity, higher tricyclic/17α-hopane ratios in most samples (1.29-7.45) may be attributed to marine influenced depositional conditions rather than maturity (Seifert and Moldowan, 1979; Philp et al., 1992).

20S/(20S+20R) isomerization ratios for C_{29}-steranes usually reach an equilibrium value of ~0.55 near the main oil generation window. While the ββ/(ββ+αα) ratio is slower to reach an equilibrium value of ~0.70 around peak oil generation, thus making it effective at higher levels of maturity (Mackenzie et al., 1980; Peters and Moldowan, 1993; Ramon and Dzou, 1999). In present study, both ratios of ββ/(ββ+αα) for 5α-C_{29} steranes and 20S/(20S+20R) for ααα-C_{29} range from 0.43-0.57 and 0.33-0.52 respectively (Table 3) indicating that these samples are at early to intermediate levels of thermal maturity.

Conclusions

The results reveal that organic matter in the Uppermost Tanezzuft Formation ('cool' shale) within Murzuq Basin is mainly Type III kerogen (gas prone) with some contribution of mixed type II and III kerogens (gas/oil prone). Generally it has poor to fair hydrocarbon potential. The predominance of C_{27} and C_{29} steranes and values of Pr/nC_{17} vs. Ph/nC_{18} in most samples indicate that organic matter in these sediments has mixed marine/terrigenous sources with a slight influence of marine input indicated by the high concentrations of tricyclic terpanes in most samples. The high values of Pr/Ph ratios and diasterane/sterane ratios, the occurrence of C_{30}-diahopane, and low values of C_{35} to C_{34} homohopanes ratios, together with low quality organic matter all suggest that these sediments were deposited in mixed oxic to sub-oxic (high Eh) conditions with hypersaline influenced sedimentation conditions.

Biomarker maturity parameters indicate that most of rock samples were generally mature (early mature to intermediate levels of maturity), as indicated by the ratios of 22S/(22S+22R), ββ/(ββ+αα), 20S/(20S+20R), and the low values of C_{30}-moretanes/C_{30}-hopanes (C_{30}βα/C_{30}αβ) ratios, together with Tmax. Therefore, it cannot be predicted that the Uppermost Tanezzuft Formation ('cool' shale) has generated significant volumes of hydrocarbons in the Murzuq Basin.

Acknowledgements

The authors would like to express their gratitude to the staff of Repsol Oil Company in Libya for providing us with shale samples. T. Hodairi is grateful to Dr. N. Fello and Dr. S. Lüning for their valuable support.

References

Aziz, A., 2000, Stratigraphy and hydrocarbon potential of the lower Palaeozoic succession of license NC 115, Murzuq Basin, S.W. Libya, *in* M.A. Sola and D. Worsley (eds.), Symposium on Geological Exploration in Murzuq Basin: Elsevier, Amsterdam, p. 349-368.

Bellini, E., and D. Massa, 1980, A stratigraphic contribution to the palaeozoic of the southern basins of Libya, *in* M.J. Salem and M.T. Busrewil (eds.), The Geology of Libya: Academic Press, London, p. 3-56.

Clark, J.P., and R.P. Philp, 1989, Geochemical characterization of evaporate and carbonate depositional environments and correlation of associated crude oils in the black Creek Basin, Alberta: Bulletin of Canadian Petroleum Geology, v. 37, p. 401-416.

Dahl, J.E., J.M. Moldowan, S.C. Teerman, M.A. McCaffrey, P. Sundararaman, M. Pena, and C.E. Stelting, 1994, Source rock quality determination from oil biomarkers I, An example from the Aspen Shale, Scully's Gap, Wyoming: AAPG Bulletin v. 78/10, p. 1507-1526.

Davidson, L., B. Simon, C. Jonathan, E. Martin, F. Andy, H. Ali, J. Jhoon, M. Bashir, and S. Jerry, 2000, The structure, stratigraphy and petroleum geology of the Murzuq Basin, southwest Libya, *in* M.S. Sola and D. Worsley (eds.), Geological Exploration in Murzuq Basin: Elsevier, Amsterdam-London-New York-Tokyo, p. 295-320.

Echikh, K., and M.A. Sola, 2000, Geology and hydrocarbon occurrences in the Murzuq Basin, S.W. Libya, *in* M.A. Sola and D. Worsley (eds.), Symposium on Geological Exploration in Murzuq Basin: Elsevier, Amsterdam, p. 175-222.

Eglinton, G., and R.J. Hamilton, 1969, Leaf epicuticular waxes: Science 156, p. 1322-1334.

ten Haven, H.L., J.W. De Leeuw, P.A. Schenck, and G.T. Klaver, 1988, Geochemistry of Mediterranean sediments, Bromine/organic carbon and uranium/organic carbon ratios as indicators for different sources of input and post depositional oxidation, respectively: Organic Geochemistry, 13/1-3, p. 255-261.

Jarvie, D.M., 1991, Total organic carbon (TOC) analysis, *in* R.K. Merrill (Ed.), Source and migration processes and evaluation techniques: N.H. Foster, and E.A. Beaumont (treatise eds.), AAPG Treatise of Petroleum Geology, Handbook of Petroleum Geology, p. 113-118.

Lijmbach, G.W.M., 1975, On the origin of petroleum: Proceedings Ninth World Petroleum Congress, Applied Sciences Publisher, London, v. 2, p. 357-369.

Lüning, S.**,** J. Craig, B. Fitches, J. Mayouf, A. Busrewil, M. El Dieb, A. Gammudi, and D.K. Loydell, 2000d, Petroleum source and reservoir rock re-evaluation in the Kufra Basin (SE Libya, NE Chad, NW Sudan), *in* M.A. Sola and D. Worsley (eds.), Geological Exploration in Murzuq Basin: Elsevier, Amsterdam, p. 151-173.

Peters, K.E., A.E. Kontorovich, and J.M. Moldowan, 1993, Geochemistry of selected oils and rocks from the central portion of the west Siberian Basin, Russia: AAPG Bulletin, v. 77, p. 863-87.

Peters, K.E., C.C. Walters, and J.M. Moldowan, 2005, The Biomarker Guide: Biomarkers and Isotopes in Petroleum Exploration and Earth History, 2nd edition: Cambridge University Press, United Kingdom, v. 2, p. 1155.

Philp, R.P., 1985, Fossil Fuel Biomarker: Elsevier Science Publishers B.V., New York, 294 p.

Philp, R.P., J.H. Chen, J.M. Fu, and G.Y. Sheng, 1992, A geochemical investigation of crude oils and source rocks from Biyang Basin, China: Organic Geochemistry, v. 18/6, p. 933-945.

Ramón, J.C., and L.I. Dzou, 1999, Petroleum geochemistry of Middle Magdalena Valley, Colombia: Organic Geochemistry, v. 30, p. 249–266.

Rullkötter, J., and R. Marzi, 1988, Natural and artificial maturation of biological markers in Toarcian shale from northern Germany, *in* L. Mattavelli and L. Novelli (eds.), Advances in Organic Geochemistry 1987: Oxford Pergamon Press, p. 639-645.

Seifert, W.K., and J.M. Moldowan, 1979, The effect of biodegradation on steranes and terpanes in crude oils, Geochimica et Cosmochimica Acta, v. 43, p. 111-126.

Sikander, A.H., S. Basu, and S.M. Rasul, 2000, Geochemical source-maturation and volumetric evaluation of lower Paleozoic source rocks in the west Libyan basins, *in* The Geology of northwest Libya, Second Symposium on the Sedimentary Basins of Libya Book of Abstracts, p. 88.

Volkman, J.K., J.R. Maxwell, 1986, Acyclic isoprenoids as biological markers, *in* R.B. Johns (ed.), Biological Markers in the Sedimentary Record: Elsevier, Amsterdam, p. 1-42.

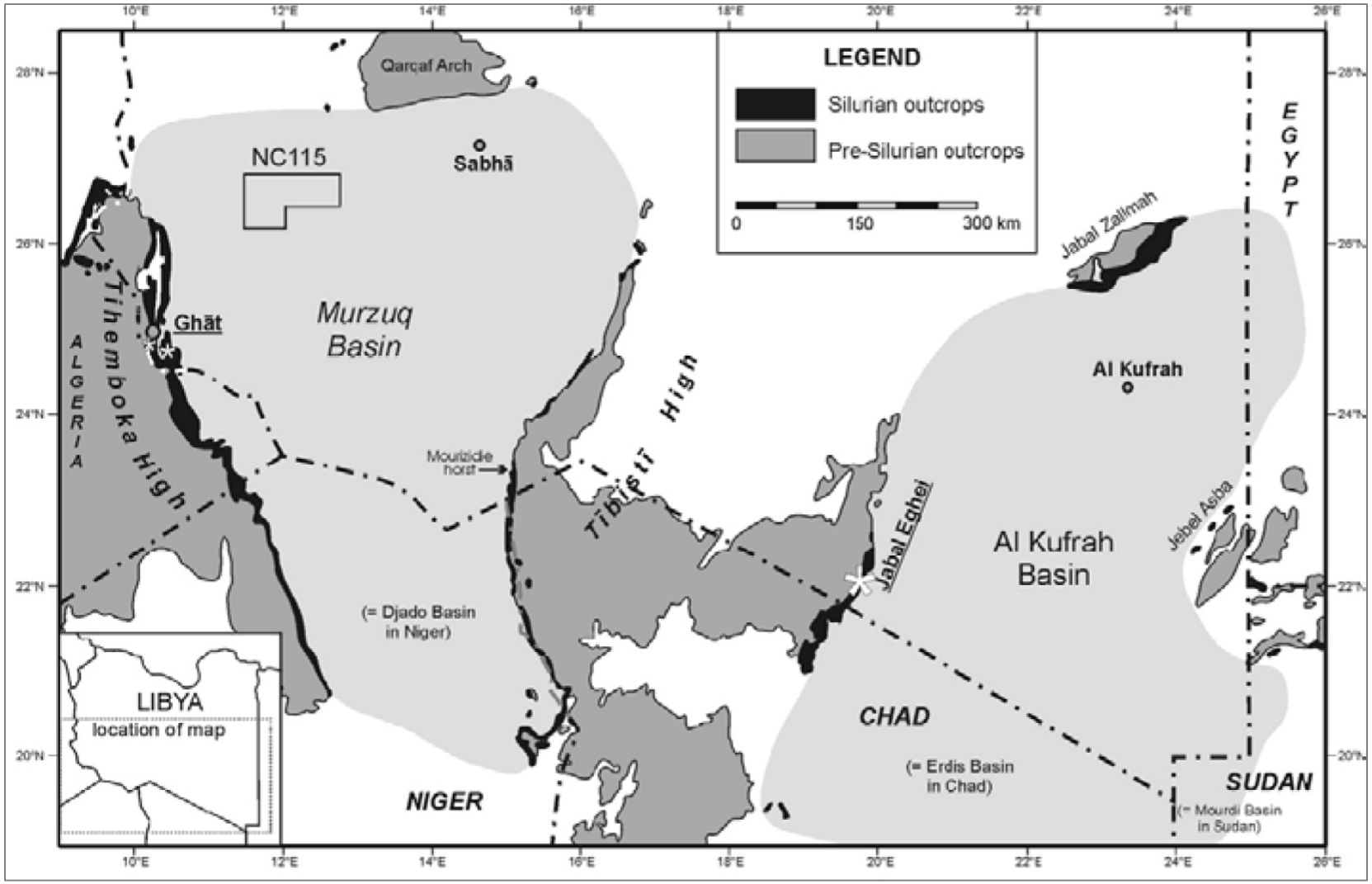

Figure 1. Location map of Murzuq Basin with position of the NC-115 Concession selected for this study. After Ghnia et al. (2008).

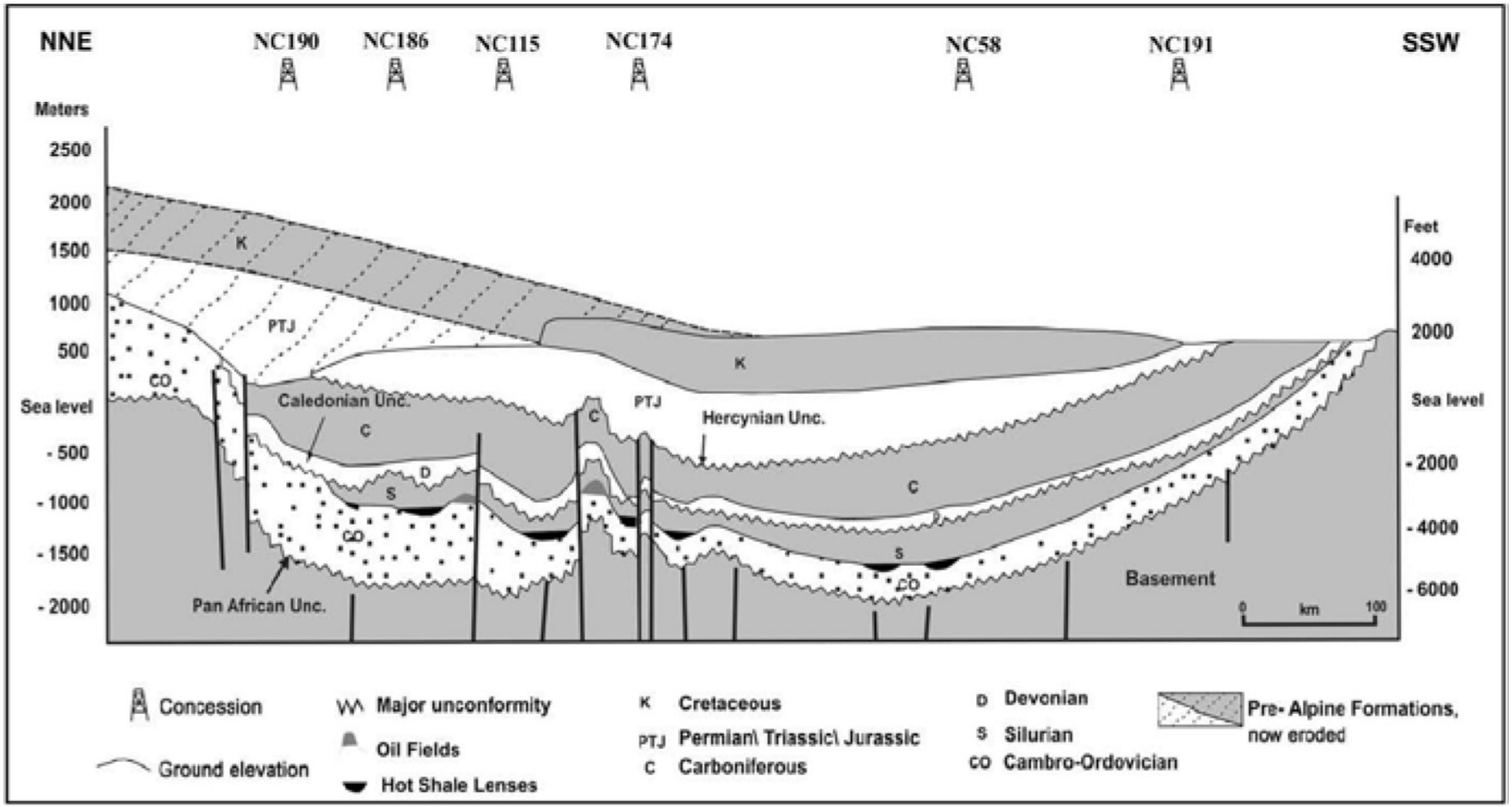

Figure 2. Schematic reconstructed cross-section showing major structures and three tectonic unconformities in the Murzuq Basin and eroded sedimentary sequences in the north. After Davidson et al. (2000).

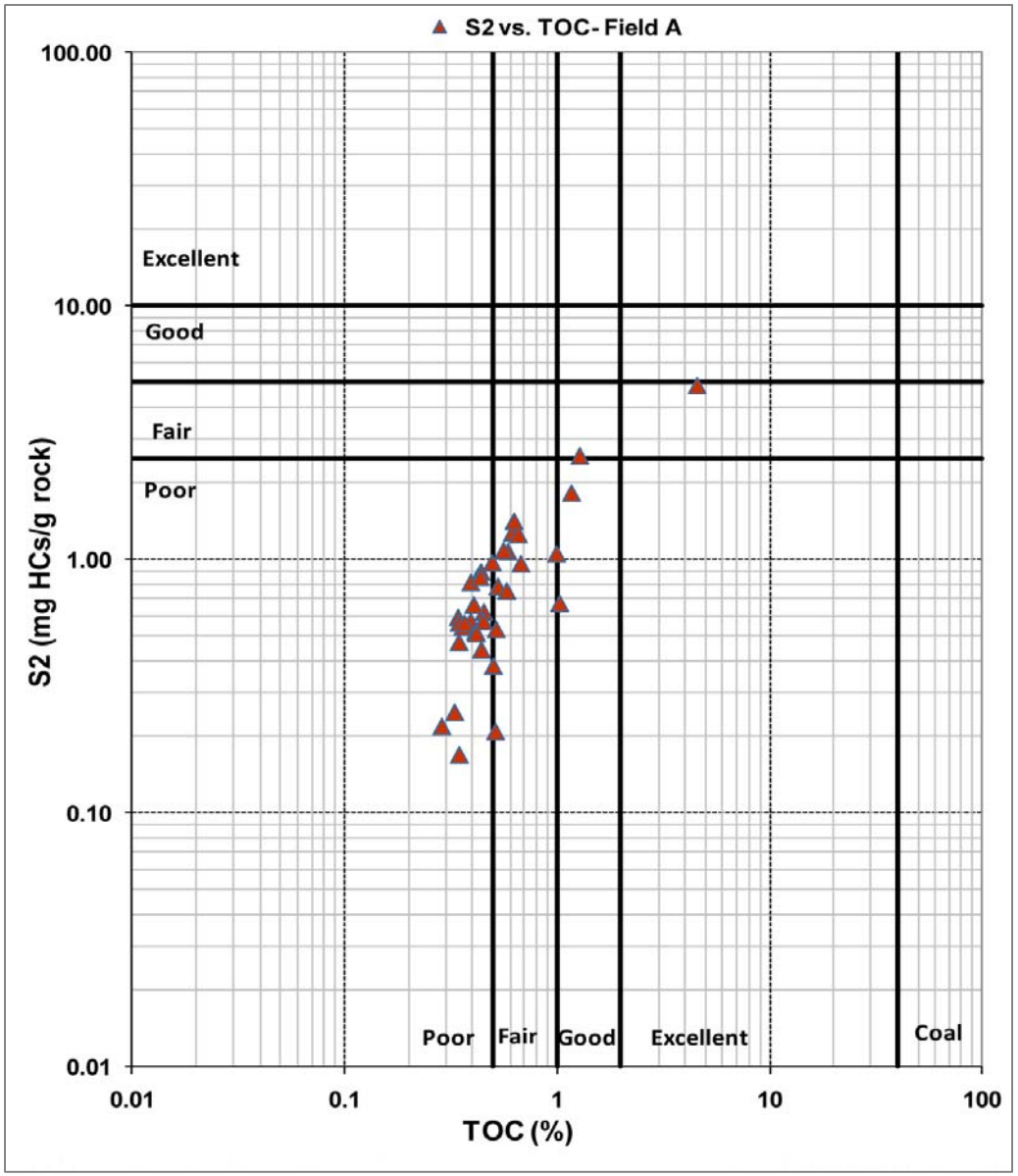

Figure 3. Crossplot showing the organic matter quantity with generally low S2 values. Tanezzuft Formation. Modified from Dembicki (2009).

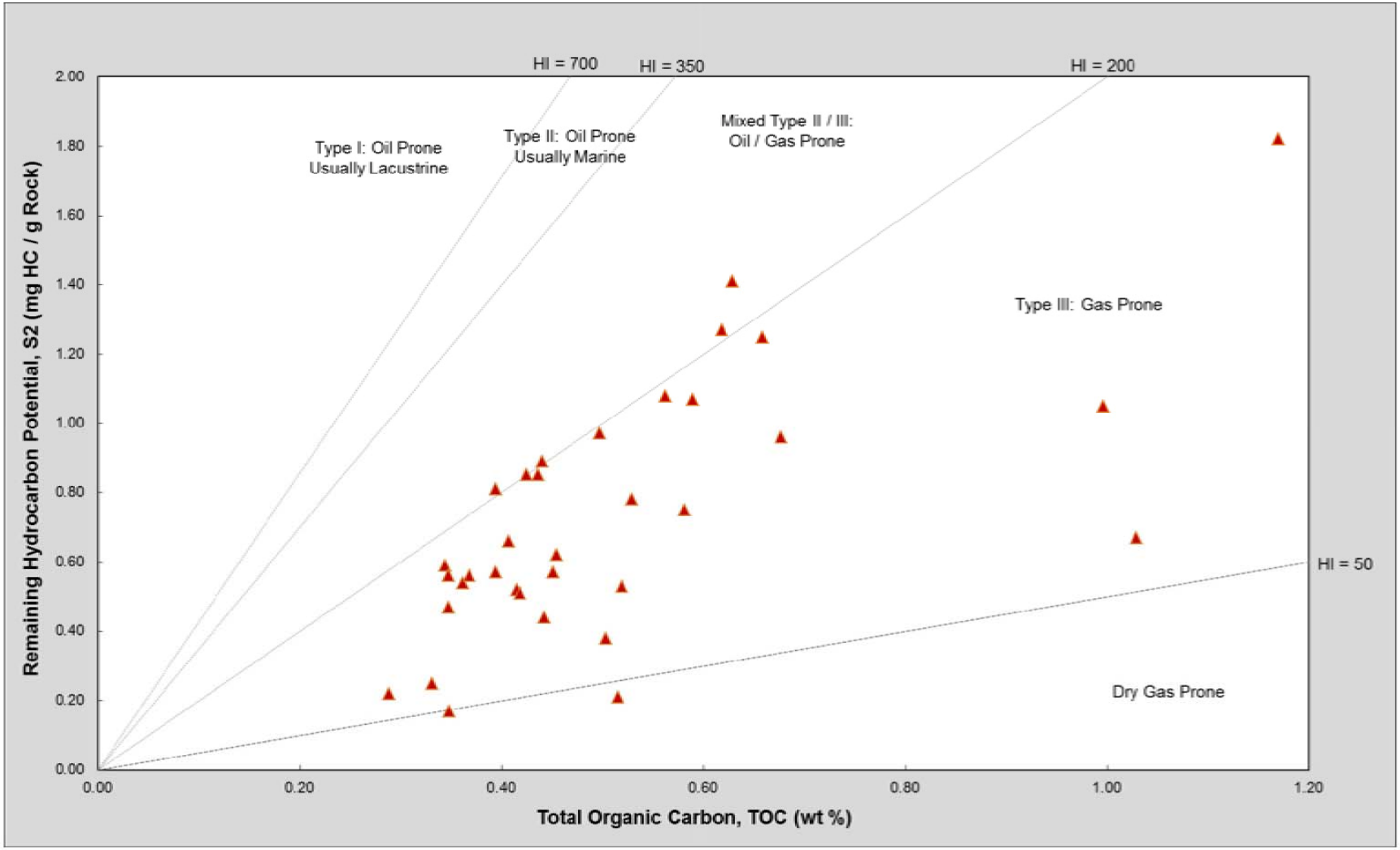

Figure 4. Crossplot between S2 mg HC/g rock and %TOC showing the organic matter quality, shales of Tanezzuft Formation, Field A, NC-115, Murzuq Basin. Modified from GeoMark Research, LTD (2009).

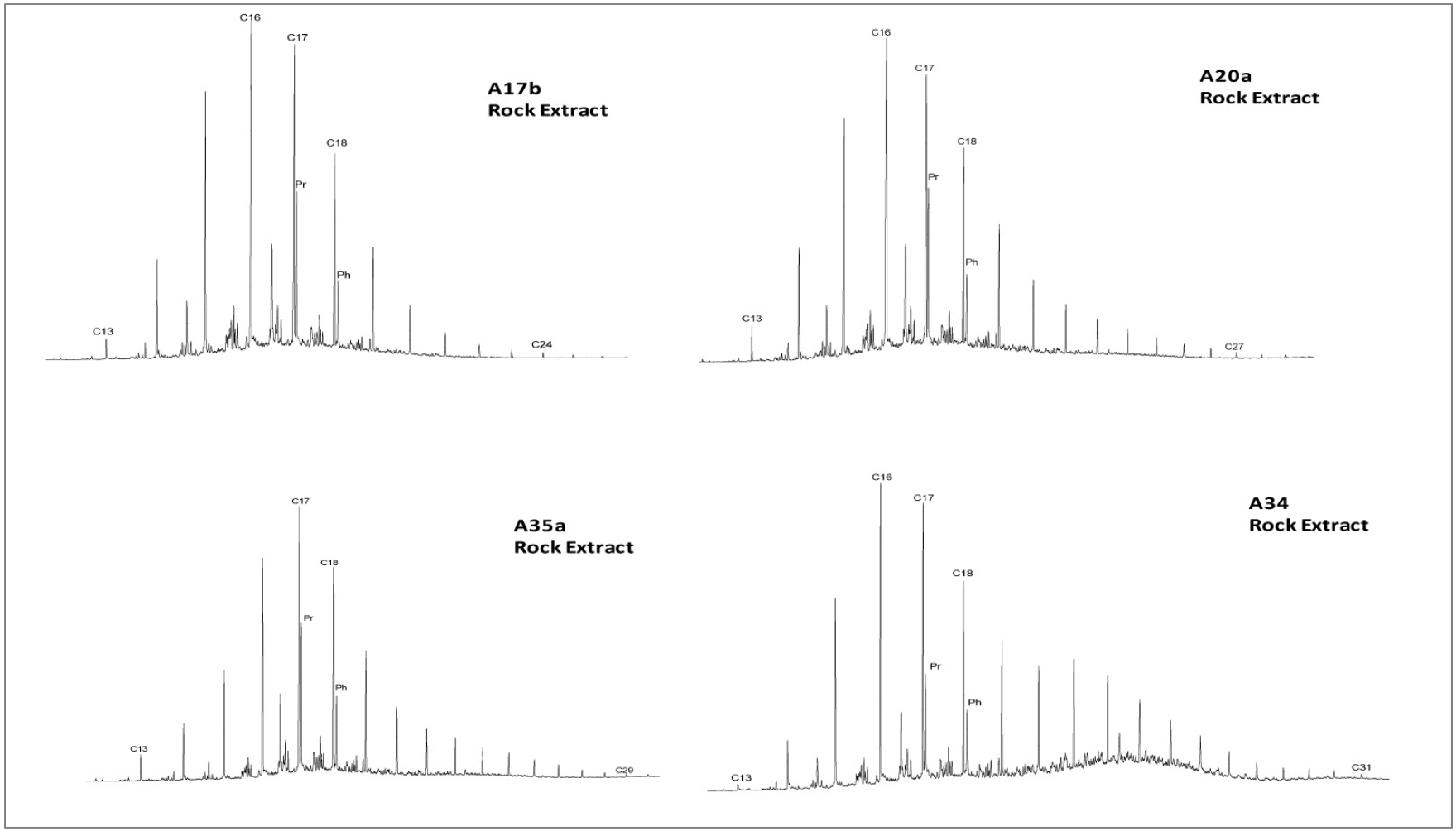

Figure 5. Gas chromatograms of aliphatic fractions showing the n-alkanes and acyclic isoprenoids for selected rock samples from Tanezzuft Formation, Murzuq Basin, NC-115, A-Field.

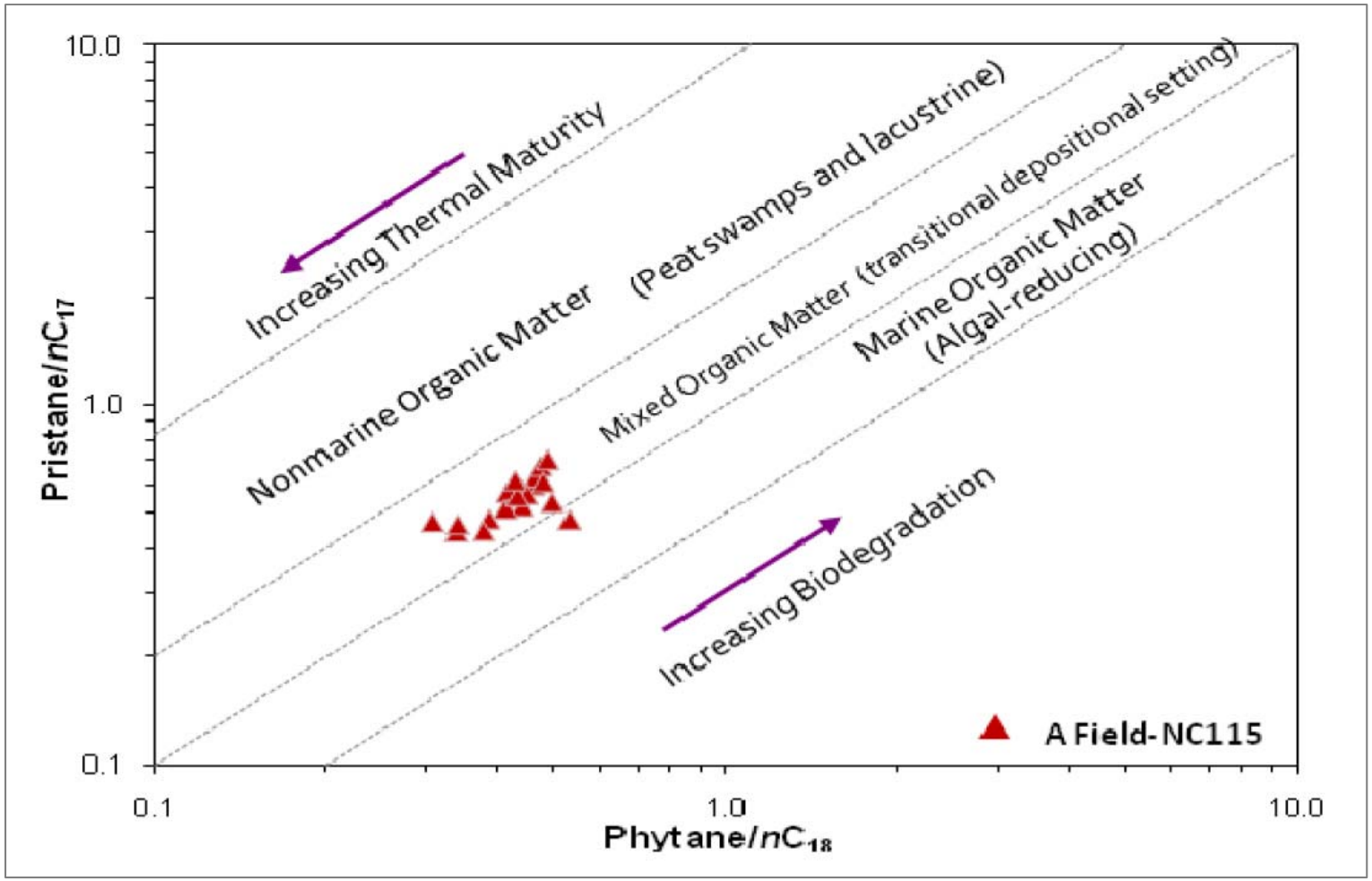

Figure 6. Isoprenoids plot of Pristane/$_{n}C_{17}$ vs. Phytane/$_{n}C_{18}$ showing redox conditions and depositional environments (Shanmugam, 1985) for samples of shales of Tanezzuft Formation, Murzuq Basin.

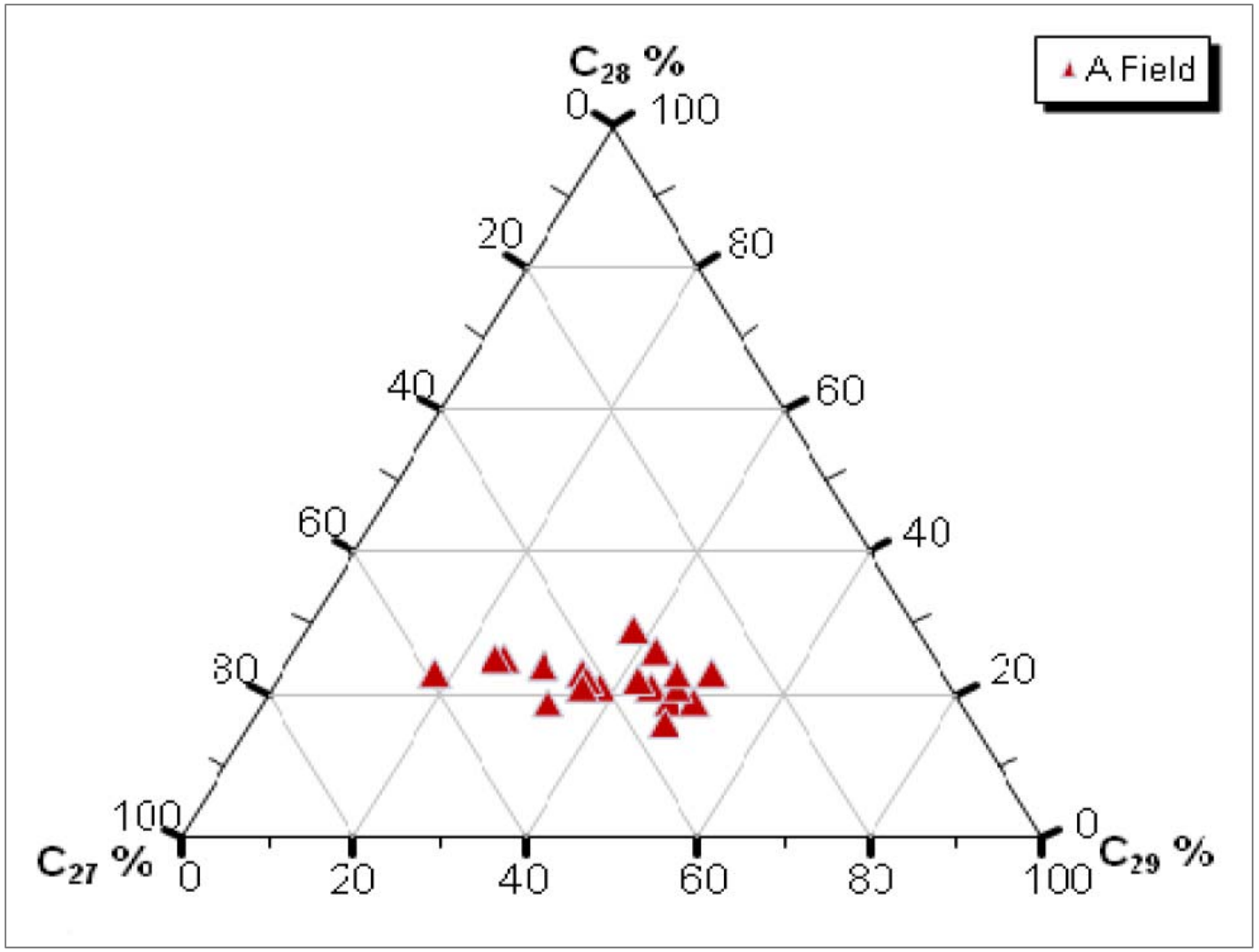

Figure 7. Ternary diagram indicating relative distributions of C_{27}, C_{28}, and C_{29} regular steranes of studied rock samples.

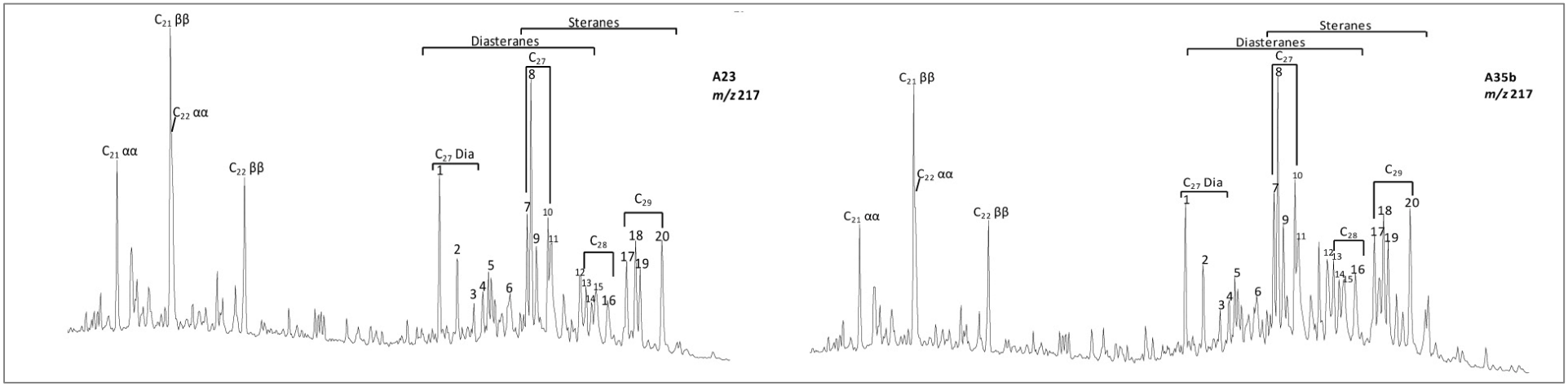

Figure 8. Mass chromatograms showing the distribution of steranes (m/z 217) of selected samples from Tanezzuft Formation, A-Field, NC-115. See Table 5 for peak identifications.

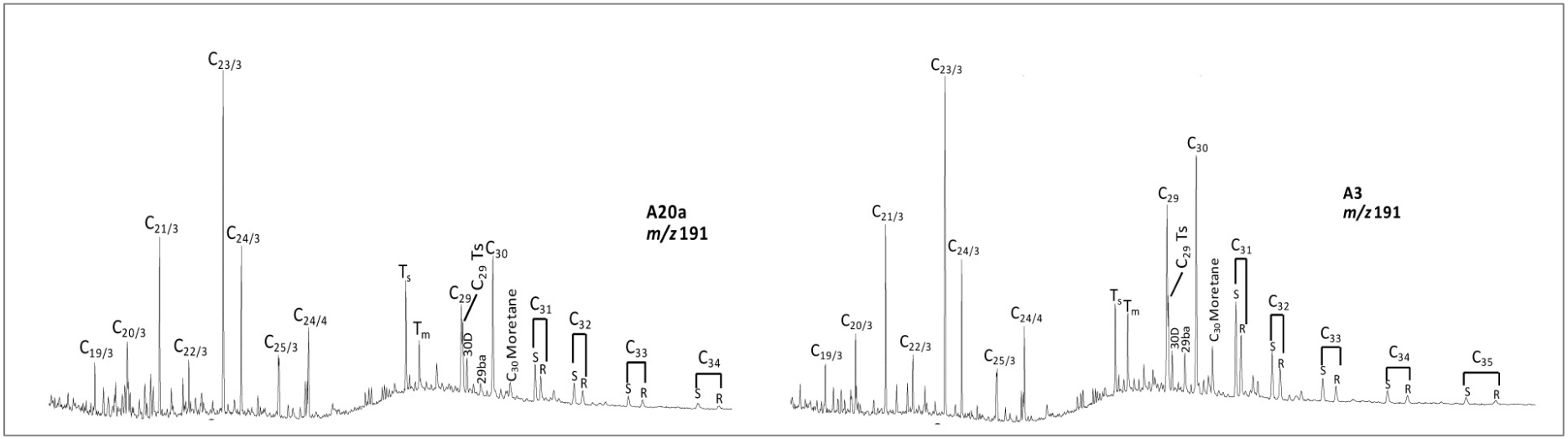

Figure 9. Mass chromatograms showing the distribution of hopanes (m/z 191) of selected rock samples from Tanezzuft Formation, Murzuq Basin, A-Field, NC-115. See Table 5 for peak identifications.

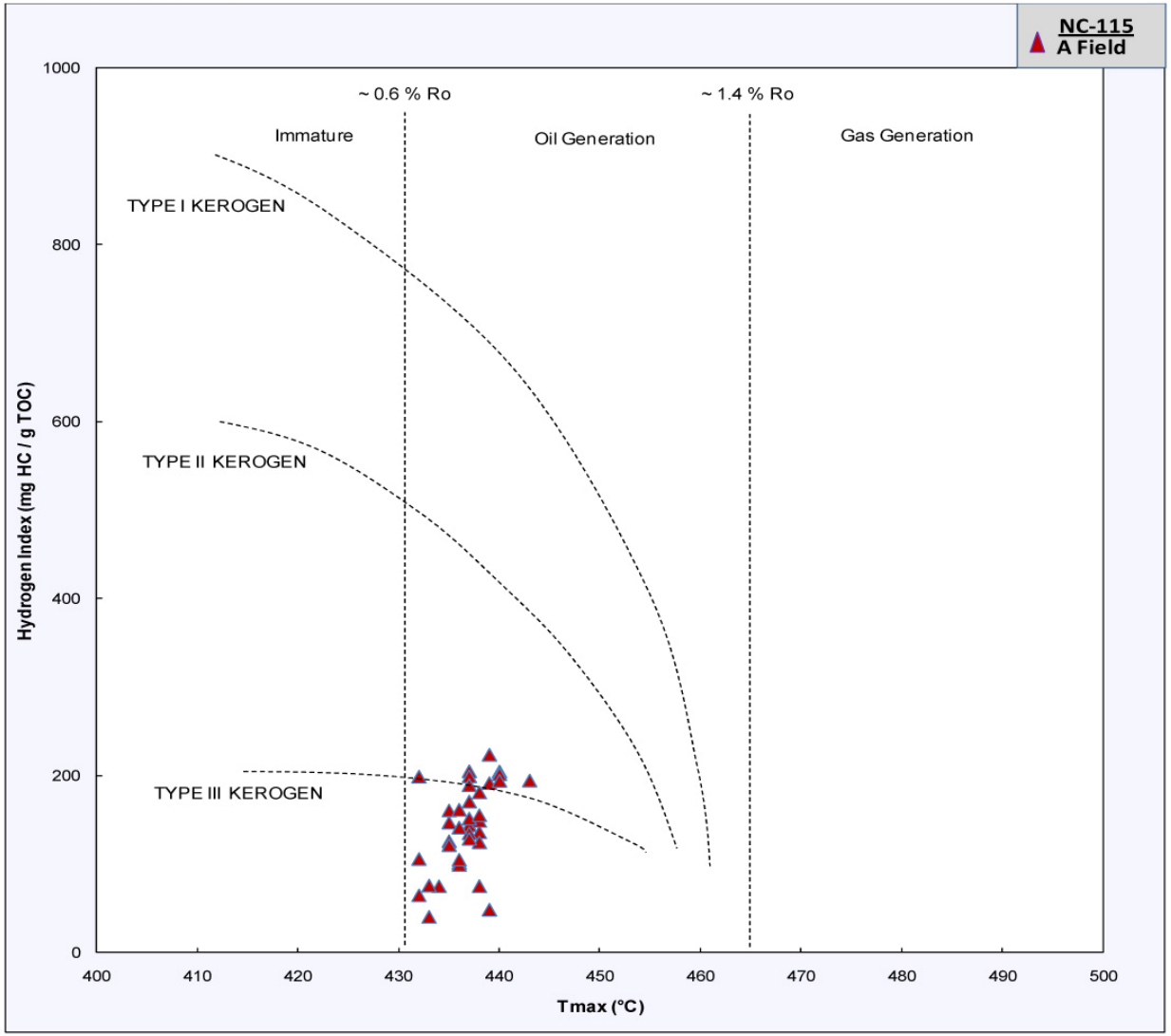

Figure 10. Tmax vs. HI plot showing maturity and kerogen type of Tanezzuft Shale samples.

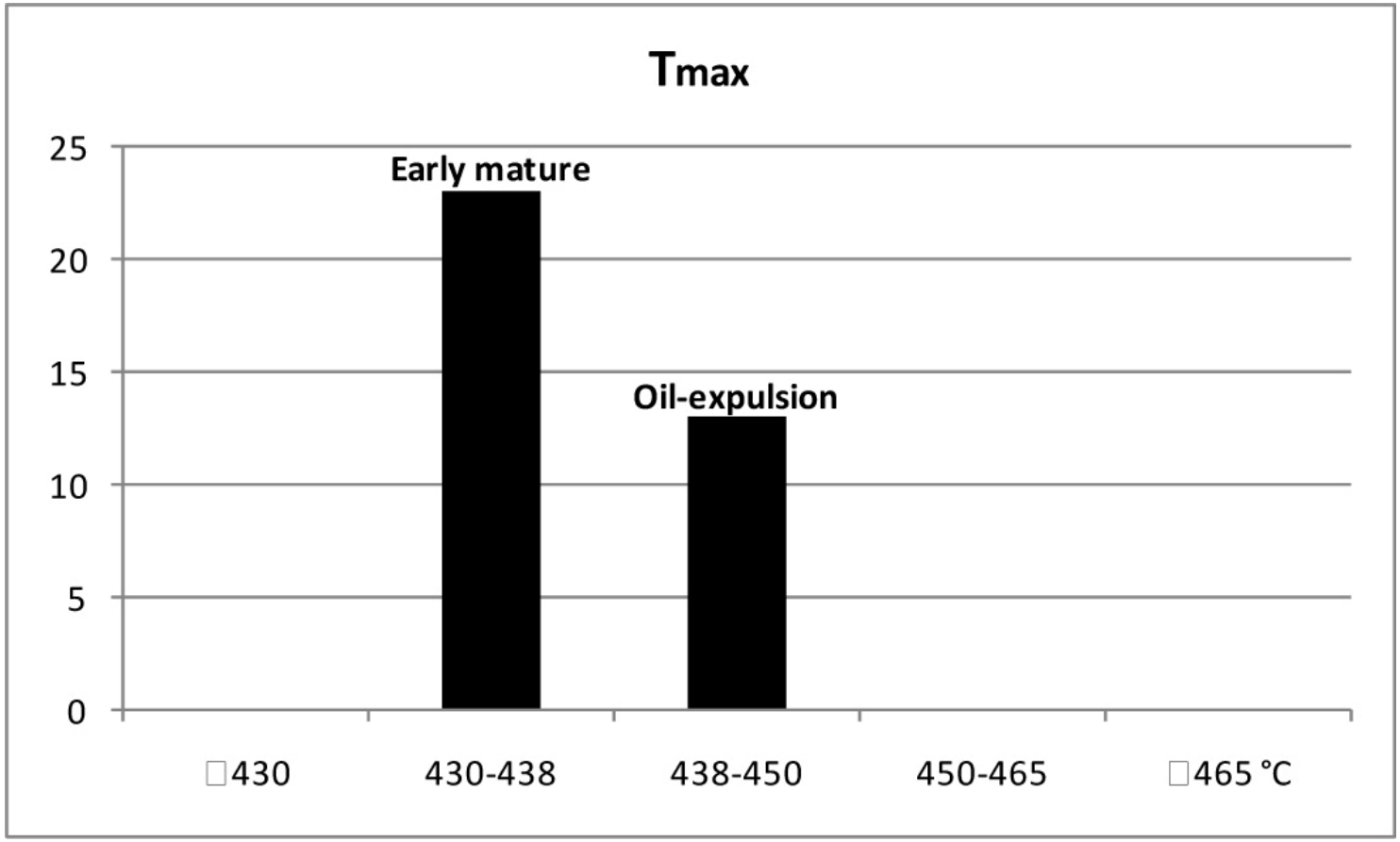

Figure 11. Showing Tmax distribution of Tanezzuft Shale samples.

Sample	Depth (ft)	TOC (wt % HC)	S1 (mg HC/g)	S2 (mg HC/g)	HI (S2x100/TOC)	PI (S1/(S1+S2)	Tmax (°C)
A6	4,915.00	0.59	0.62	1.07	181	0.37	438
A6a	4,810.00	1.28	10.89	2.55	199	0.81	432
A10	4,858.00	0.50	0.93	0.36	75	0.71	438
A16	4,400.00	0.35	0.49	0.56	161	0.47	435
A17a	4,370.00	0.58	0.47	0.78	147	0.55	435
A17b	4,380.00	0.52	0.41	0.58	102	0.44	439
A18	4,200.00	0.45	0.58	0.57	128	0.48	435
A19a	4,200.00	0.68	0.96	0.99	142	0.26	439
A20a	4,545.00	0.86	0.49	1.25	190	0.27	437
A22	4,800.00	0.58	0.50	0.75	129	0.40	437
A23	4,180.00	1.08	0.59	0.67	65	0.47	432
A59	4,870.00	0.40	0.26	0.81	205	0.24	440
A64	4,730.00	0.56	1.08	1.08	192	0.49	439
A65a	4,840.00	0.50	0.82	0.97	195	0.39	448
A65b	4,800.00	0.69	0.28	1.41	224	0.14	439
A67a	5,010.00	1.17	1.27	1.82	158	0.41	436
A67b	4,370.00	0.44	0.51	0.85	195	0.58	440

TOC: total organic carbon (%); HI: hydrogen index; PI: production index; Tmax: maximum pyrolysis temperature.

Table 1. Result of Rock Eval analyses of selected samples from Tanezzuft Formation, Murzuq Basin.

Sample ID	Lithology	Range	n-alkane Maximum	Pr/Ph	Pr/nC_{17}	Ph/nC_{18}	nC_{17}/nC_{25}	$Pr+nC_{17}/Ph+nC_{18}$	CPI
A3	Shale	nC13-nC27	nC16	1.56	0.53	0.49	28.45	1.49	1.24
A5	Shale	nC13-nC27	nC14	1.71	0.47	0.38	43.10	1.47	1.38
A6a	Shale	nC16-nC27	nC19	0.82	0.56	0.41	2.50	0.67	1.86
A6b	Shale	nC15-nC26	nC19	0.96	0.57	0.43	8.68	0.79	1.60
A10	Shale	nC14-nC24	nC17	1.68	0.59	0.46		1.43	
A17a	Shale	nC13-nC26	nC16	2.26	0.62	0.46	58.72	1.86	1.42
A17b	Shale	nC13-nC24	nC16	1.98	0.52	0.43	93.74	1.76	
A18	Shale	nC13-nC26	nC16	2.21	0.67	0.47	72.44	1.77	1.15
A19a	Shale	nC13-nC27	nC16	1.93	0.56	0.45	52.91	1.68	1.55
A19b	Shale	nC13-nC27	nC16	1.58	0.44	0.37	34.26	1.41	1.48
A20a	Shale	nC13-nC27	nC16	2.32	0.69	0.49	29.91	1.85	1.15
A20b	Shale	nC13-nC27	nC17	1.84	0.60	0.48	41.16	1.58	1.24
A21	Shale	nC13-nC27	nC16	2.10	0.44	0.33	67.42	1.73	1.18
A22	Shale	nC12-nC27	nC16	2.14	0.47	0.30	16.43	1.57	1.12
A23	Shale	nC12-nC27	nC17	1.79	0.51	0.41	29.05	1.54	1.19
A34	Shale	nC13-nC31	nC16	1.23	0.47	0.53	6	1.32	1.24
A35a	Shale	nC13-nC30	nC17	1.83	0.55	0.43	19.21	1.55	1.16
A35b	Shale	nC12-nC32	nC17	1.93	0.46	0.34	5.93	1.55	1.12
A37a	Shale	nC13-nC25	nC15	2.23	0.61	0.42	39.70	1.758	

Table 2. Gas chromatogram data of n-alkanes and acyclic isoprenoids from Tanezzuft Formation, Murzuq Basin.

Pr: pristane; Ph: phytane; CPI: Carbon Preference Index was calculated based on Bray and Evans (1961) Formula:

$$CPI = 1/2 \left[\frac{C_{25}+C_{27}+C_{29}+C_{31}+C_{33}}{C_{26}+C_{28}+C_{30}+C_{32}+C_{34}} + \frac{C_{25}+C_{27}+C_{29}+C_{31}+C_{33}}{C_{24}+C_{26}+C_{28}+C_{30}+C_{32}} \right]$$

Samples	Steranes[a]			Diasteranes/steranes[b]	C29[c]	C29[d]	C27/C29[e]	Preg/(preg+ster+dias)[f]
	C27 %	C28 %	C29 %		ββ/(ββ+αα)	20S/(20S+20R)		
A3	35	21	44	0.6	0.43	0.41	0.8	0.6
A5	34	19	47	1	0.47	0.39	0.72	0.64
A6b	46	24	30	2.2	0.57	0.47	1.56	0.85
A10	46	24	30	1.3	0.49	0.44	1.53	0.82
A17a	27	23	50	1.5	0.55	0.43	0.53	0.63
A17b	31	19	50	1.6	0.45	0.42	0.62	0.73
A18	41	21	38	1.1	0.45	0.4	1.08	0.76
A19a	42	23	35	0.9	0.55	0.44	1.17	0.79
A19b	32	21	47	1.5	0.51	0.33	0.66	0.73
A20a	36	22	42	1.5	0.52	0.41	0.85	0.67
A20b	42	22	36	0.8	0.51	0.4	1.17	0.72
A21	31	23	46	2	0.51	0.37	0.67	0.67
A22	36	16	48	1.8	0.54	0.4	0.74	0.47
A23	32	26	42	0.8	0.44	0.45	0.75	0.58
A34	51	25	24	0.6	0.52	0.49	2.13	0.72
A35a	48	19	33	0.8	0.53	0.37	1.44	0.64
A35b	33	29	38	0.5	0.44	0.44	0.85	0.51
A37a	59	23	18	0.6	0.54	0.52	3.17	0.73
A37b	43	21	36	1.4	0.54	0.41	1.2	0.72

Table 3. Sterane parameters (m/z 217 chromatograms) of rock samples from A-Field, Murzuq Basin.

[a]5α(H),14α(H),17α(H)-20R-Steranes, [b]13β(H),17α(H),20(R)-cholestane (C27-diasterane)/5α(H),14α(H),17α(H),20(R)-cholestane (C27-Regular sterane), [C]5α(H),14β(H),17β(H)/[5α(H),14β(H),17β(H) + 5α(H),14α(H),17α(H)] for C29-Steranes, [d]calculated for C29-5α (H),14α(H),17α(H)-Steranes, [e]5α (H),14α(H),17α(H)-20R-Steranes, [f][5α (H),14β (H),17β(H) –Pregnane + 5α(H),14β(H),17β(H) –Homopregnane]/ [5α(H),14β(H),17β(H),20(R)-cholestane + pregnane + homopregnane +13β(H),17α(H),20(S)-diacholestane].

Samples	Ts/(Ts+Tm) [a]	C_{19}/C_{23} [b]	22S/(22S+22R) [c]	HHI [d]	$C_{30}\beta\alpha/C_{30}\alpha\beta$ [e]	C_{24}/C_{30} [f]	C_{23}/C_{30} [g]	C_{23}/C_{29} [h]	Tris/17α-hop [i]	$C_{30}d/C_{29}Ts$ [j]
A3	0.45	0.2	0.56	0.65	0.23	0.2	0.76	1.14	0.66	0.58
A5	0.6	0.36	0.57	0.58	0.35	0.27	0.7	1.05	0.64	0.53
A6b	0.51	0.2	0.53	□	0.13	0.46	7.59	10.48	7.45	0.67
A10	0.52	0.27	0.51	□	0.29	1.42	6.57	5.72	5.27	0.93
A17a	0.65	0.55	0.55	0.6	0.18	0.22	0.64	1.09	0.84	0.68
A17b	0.65	0.44	0.54	□	0.21	0.41	1.02	1.39	1.29	0.22
A18	0.53	0.41	0.6	□	0.22	0.39	1.32	1.83	1.54	0.54
A19a	0.54	0.24	0.63	□	0.16	0.52	2.13	2.7	2.11	0.53
A19b	0.57	0.32	0.58	0.39	0.16	0.26	0.7	1.14	0.83	0.39
A20a	0.53	0.19	0.57	0.42	0.13	0.4	1.41	2.61	1.32	0.54
A20b	0.44	0.14	0.57	0.57	0.17	0.47	1.88	1.98	1.36	0.83
A21	0.56	0.28	0.6	□	0.13	0.49	1.81	2.25	1.95	0.63
A22	0.6	0.29	0.59	0.51	0.23	0.34	1	1.78	0.97	0.76
A23	0.47	0.11	0.57	0.5	0.21	0.17	0.95	1.09	0.75	0.53
A34	0.42	0.04	0.58	□	0.11	0.75	4.25	4.46	3.22	0.49
A35a	0.61	0.13	0.48	0.93	0.19	0.57	3.028	3.47	2.38	1.49
A35b	0.57	0.21	0.57	0.34	0.2	0.14	0.22	0.33	0.22	0.24
A37a	0.56	0.06	0.75	□	0.21	1.77	8.8	6.83	4.94	0.99
A37b	0.7	0.1	0.61	□	0.18	0.73	3.9	6.56	3.27	1.17

Table 4. Hopane indices of rock samples measured on the m/z 191, Tanezzuft Formation, NC-115, A-Field, Murzuq Basin.

[a]18α (H)-22,29,30-trisnorneohopane/(18α (H)-22,29,30-trisnorneohopane + 17α (H)-22,29,30-trisnorhopane), [b]$C_{19}H_{34}$ tricyclic terpane/ $C_{23}H_{42}$ tricyclic terpane, [c]17α(H), 21β(H), 22(S)-bishomohopane/(17α(H), 21β(H), 22(S)-bishomohopane+17α(H), 21β(H), 22(R)-bishomohopane): for C_{32}homohopane, [d]Homohopane Index; 17α(H), 21β(H), 22(S+R)-pentakishomohopane/(17α(H), 21β(H), 22(S+R)- tetrakishomohopane (C35/C34 homohopanes), [e]17β (H), 21α (H)-hopane (moretane)/ 17α(H), 21β(H)-hopane, [f]$C_{24}H_{44}$ tetracyclic terpane/17α(H), 21β(H)-hopane, [g]$C_{23}H_{42}$ tricyclic terpane/17α(H), 21β(H)-hopane, [h]$C_{23}H_{42}$ tricyclic terpane/17α(H), 21β(H)-30-norhopane, [i]tricyclic terpanes/17α -hopanes: [C19+C20+C21+C22+C23+C24+C25]/[17α (H)-22,29,30-trisnorhopane + 17α(H), 21β(H)-30-norhopane + 17α(H), 21β(H)-hopane + 17α(H), 21β(H), 22(S+R)-homohopane + 17α(H), 21β(H), 22(S+R)-bishomohopane + 17α(H), 21β(H), 22(S+R)-trishomohopane + 17α(H), 21β(H), 22(S+R)- tetrakishomohopane + 17α(H), 21β(H), 22(S+R)-pentakishomohopane], [j]15α-methyl-17α(H)-27-norhopane/18α (H)-30-norneohopane.

Peak I.D.	STERANES (*m/z* 217)	Peak I.D.	COMPOUNDS (*m/z* 191)
21αα	Diapregnane	C19/3	C19 Tricyclic Terpane
21ββ	5α(H),14β(H),17β(H)- pregnane	C20/3	C20 Tricyclic Terpane
22αα	Diahomopregnane	C21/3	C21 Tricyclic Terpane
22ββ	5α(H),14β(H),17β(H)-homopregnane	C23/3	C23 Tricyclic Terpane
1	13β(H),17α(H),20(S)-cholestane (diasterane)	C24/3	C24 Tricyclic Terpane
2	13β(H),17α(H),20(R)-cholestane (diasterane)	C25/3	C25 Tricyclic Terpane
3	13α(H),17β(H),20(S)-cholestane (diasterane)	C24/4	C24 Tetracyclic Terpane
4	13α(H),17β(H),20(R)-cholestane (diasterane)	Ts	C27 18α (H)-22,29,30-trisnorneohopane (Ts)
5	24-methyl-13β(H),17α(H),20(S)-cholestane (diasterane)	Tm	C27 17α (H)-22,29,30-trisnorhopane (Tm)
6	24-methyl-13β(H),17α(H),20(R)-cholestane (diasterane)	C29αβ	C29 17α (H),21β(H)-30-norhopane
7	5α(H),14α(H),17α(H),20(S)-cholestane + 24-methyl-13α(H),17β(H),20(S)-cholestane (diasterane)	C29 Ts	C29 Ts 18α(H)-30-norneohopane
8	5α(H),14β(H),17β(H),20(R)-cholestane + 24-ethyl-13β(H),17α(H),20(S)-cholestane (diasterane)	30D	15α-methyl-17α(H)-27-norhopane (diahopane)
9	5α(H),14β(H),17β(H),20(S)-cholestane + 24-methyl-13α(H),17β(H),20(R)-cholestane (diasterane)	29βα	17β (H), 21α (H)-30-norhopane (normoretane)
10	5α(H),14α(H),17α(H),20(R)-cholestane	C30αβ	C30 17α (H),21β(H)-hopane
11	24-ethyl-13β(H),17α(H),20(R)-cholestane (diasterane)	C30M	C30 17β (H),21α (H)-moretane
12	24-ethyl-13α(H),17β(H),20(S)-cholestane (diasterane)	C31αβS	C31 17α (H),21β(H)-30-homohopane (22S & 22R)
13	24-methyl-5α(H),14α(H),17α(H),20(S)-cholestane	C32αβS	C32 17α (H),21β (H)-30-bishomohopane (22S & 22R)
14	24-methyl-5α(H),14β(H),17β(H),20(R)-cholestane + 24-ethyl-13α(H),17β(H),20(R)-cholestane (diasterane)	C33αβS	C33 17α (H),21 β (H)-30-trishomohopane (22S & 22R)
15	24-methyl-5α(H),14β(H),17β(H),20(S)-cholestane	C34αβS	C34 17α (H),21 β (H)-30-tetrakishomohopane (22S & 22R)
16	24-methyl-5α(H),14α(H),17α(H),20(R)-cholestane	C35αβS	C35 17α (H),21 β (H)-30-pentakishomohopane (22S & 22R)
17	24-ethyl-5α(H),14α(H),17α(H),20(S)-cholestane		
18	24-ethyl-5α(H),14β(H),17β(H),20(R)-cholestane		
19	24-ethyl-5α(H),14β(H),17β(H),20(S)-cholestane		
20	24-ethyl-5α(H),14α(H),17α(H),20(R)-cholestane		

Table 5. Steranes (m/z 217) and Tetracyclic and Pentacyclic Terpanes (m/z 191) identification in chromatograms of Figures 8 and 9, based on Philp (1985) and Peters and Moldowan (1993).